# A Numerical Simulation of Dryline Sensitivity to Soil Moisture

LEWIS D. GRASSO

*Cooperative Institute for Research in the Atmosphere, Fort Collins, Colorado*

(Manuscript received 25 June 1999, in final form 3 December 1999)

ABSTRACT

Previous studies have explained dryline movement to be a result of vertical turbulent mixing. Such mixing was shown to efficiently erode the western edge of the shallow moist layer above sloping terrain.

Two- and three-dimensional simulations have been used to demonstrate the impact of surface physiography on dryline evolution. Those simulations included changes in vegetation type, vegetation coverage, and soil moisture. In particular, dryline morphology has been shown to be dependent on the horizontal distribution of soil moisture. Modeling studies have also suggested that increases in the low-level horizontal water vapor gradient, associated with a dryline, are a result of frontogenetic forcing. The current study will extend past results by including more sensitivity experiments showing the dependence of dryline morphology on soil moisture.

In this paper, the Regional Atmospheric Modeling System was used to simulate the 26 April 1991 central plains dryline. Five simulations were conducted in which only soil moisture was varied. Results suggest that the movement of the dryline and the magnitude of the low-level water vapor gradient are sensitive to changes in soil moisture. Results from the constant soil moisture case show little movement of the 9.0 g kg$^{-1}$ water vapor mixing ratio isohume during the day. In that simulation the low-level horizontal gradient of water vapor displayed little change with time.

Simulated dryline evolution can be viewed as a two-step process. The first is the apparent eastward movement of drier air due to turbulent erosion of the shallow moist layer. The second step is the relatively rapid increase of the low-level horizontal gradient of water vapor. The increase of the gradient was found to be in response to vertically oriented thermally driven solenoids and frontogenetic forcing.

## 1. Introduction

The dryline is of particular meteorological interest to both weather forecasters and the general public because it is a region where severe and tornadic thunderstorms can form (Rhea 1966; Bluestein and Parker 1993). These thunderstorms also produce rain for agricultural regions of the central plains. Typically drylines are regions where thunderstorms develop in the spring and early summer.

A dryline in the central plains of the United States is generally a north–south-oriented boundary that has an eastward gradient of water vapor in the lowest few kilometers above the ground (McGuire 1962; Schaefer 1986). A consistent definition of a dryline boundary is lacking as previous studies indicate. Many methods have been used to define the location of the dryline. Koch and McCarthy (1982) used the 355-K isopleth of equivalent potential temperature ($\theta_e$). Schaefer (1974) used the 9.0 g kg$^{-1}$ water vapor mixing ratio ($r_v$) isohume, while Rhea (1966) used the first organized line of veering winds from the 3-hourly synoptic surface charts. As a result of this, references made about the location of a dryline relative to other processes, such as the development of thunderstorms, may vary from one study to the next.

The low-level horizontal gradient of water vapor is not always associated with a dryline. Early morning gradients are usually rather small, while in the afternoon dewpoint gradients of several degrees Celsius per kilometer have been observed to develop rapidly (Parsons et al. 1991; Ziegler and Hane 1993; Hane et al. 1993). In this paper the simulated dryline will be denoted as the region where the magnitude of the low-level $\nabla_h r_v$ increases rapidly in the afternoon and this region is embedded within a larger-scale moisture gradient. Understanding the mechanism that forms the relatively large eastward moisture gradient has been a research topic for many years.

In the early morning, the thickness of the moist layer associated with the dryline decreases toward the west due to the increase in elevation of the terrain in the central plains. Daytime heating has been suggested as a factor in the erosion of the shallow moist layer by vertical mixing. This gives the appearance that the dryline (defined as the 9.0 g kg$^{-1}$ isohume) moves rapidly

*Corresponding author address:* Dr. Lewis D. Grasso, NOAA/NESDIS/RAMMT CIRA, Colorado State University, West Laporte Avenue, Fort Collins, CO 80523.
E-mail: grasso@cira.colostate.edu

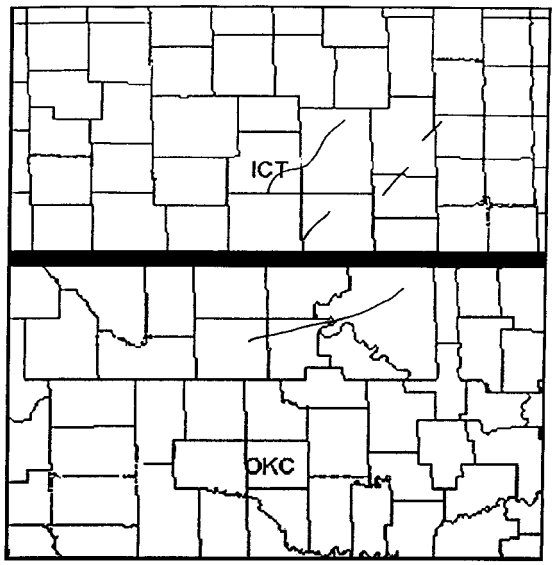


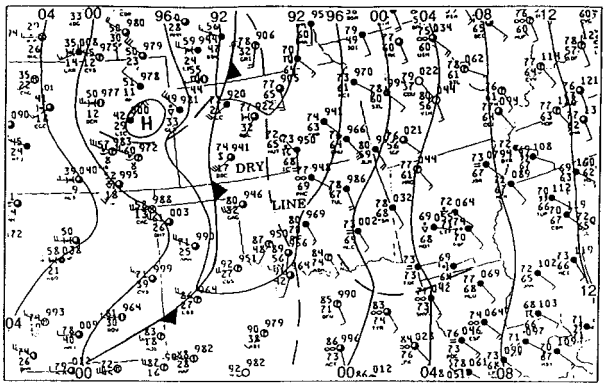


FIG. 1. Tornado tracks superimposed on a county map of northern Oklahoma and southern Kansas. Wichita, KS, is denoted by ICT and Oklahoma City by OKC. The surface analysis from 26 Apr 1991 at 2300 UTC is also shown.

eastward as the moisture gradient increases (Schaefer 1974). An observational study of the 8 June 1974 Oklahoma dryline revealed that wavelike perturbations propagated along the dryline (defined as the 355-K $\theta_e$ contour) and contributed more to its eastward motion than the downward slope of the terrain (McCarthy and Koch 1982).

Solenoidal circulations, in response to horizontal virtual potential temperature gradients, have been proposed to cause an increases in the eastward moisture gradient through horizontal convergence at the dryline (Ogura and Chen 1977; Anthes et al. 1982; Benjamin 1986; Sun and Wu 1992; Ziegler et al. 1995). In a two-dimensional simulation of the 24 May 1989 dryline in western Oklahoma, Ziegler et al. (1995) showed that the water vapor field experienced frontogenesis.

Past work has demonstrated the importance of horizontally varying soil moisture on dryline morphology.

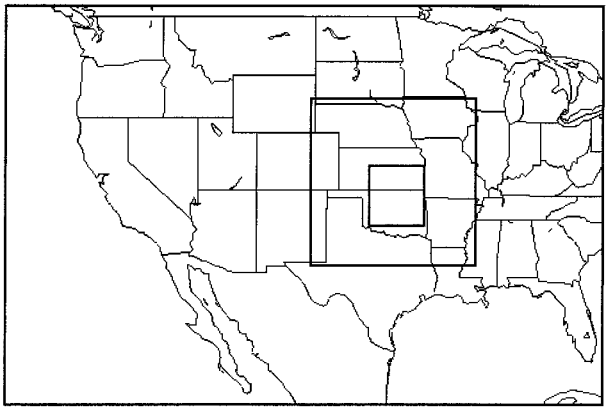

FIG. 2. Location of the three two-way interactive grids used for this study.

The Pennsylvania State University–National Center for Atmospheric Research (NCAR) Mesoscale Model was used by Lanicci et al. (1987) to examine the influence of soil moisture on a simulated dryline. In their simulations the horizontal and vertical grid spacings were relatively large. Results suggested that variations in soil moisture produced a significant effect on the horizontal water vapor gradient on the scale of 100 km. Based on observed drylines, Ziegler et al. (1995) used horizontal grid spacings of 5 km in their two-dimensional simulations. Their results suggested that horizontally varying soil moisture was necessary for the formation of the simulated dryline. No dryline formed in the simulation with horizontally constant soil moisture. Shaw et al. (1997) demonstrated the importance of surface characteristics on dryline evolution. They showed that horizontal gradients in soil moisture and vegetation type were important for dryline intensification. Specifically, they found that horizontally constant soil moisture would increase/decrease sensible/latent heat fluxes, compared to variable soil moisture, east of the future location of the dryline. They showed that a simulation with constant soil moisture had a negative impact on dryline formation in that the eastward water vapor gradient was much smaller compared to observations and a simulation that included variable soil moisture.

This paper presents the results of a study that extends previous work on dryline morphology relative to soil moisture by providing more sensitivity experiments. The methodology was to run multiple simulations of dryline evolution in which only the initial, horizontally varying, soil moisture was changed. The Regional Atmospheric Modeling System (RAMS) mesoscale model was used and initialized at 1200 UTC 26 April 1991. All simulations were 12h long and terminated at 0000 UTC 27 April 1991. Results show that dryline formation varied with changes in the initial horizontal profile of soil moisture. This suggests that the formation of some drylines may depend on the history of past precipitating events. A simulation with horizontally constant soil

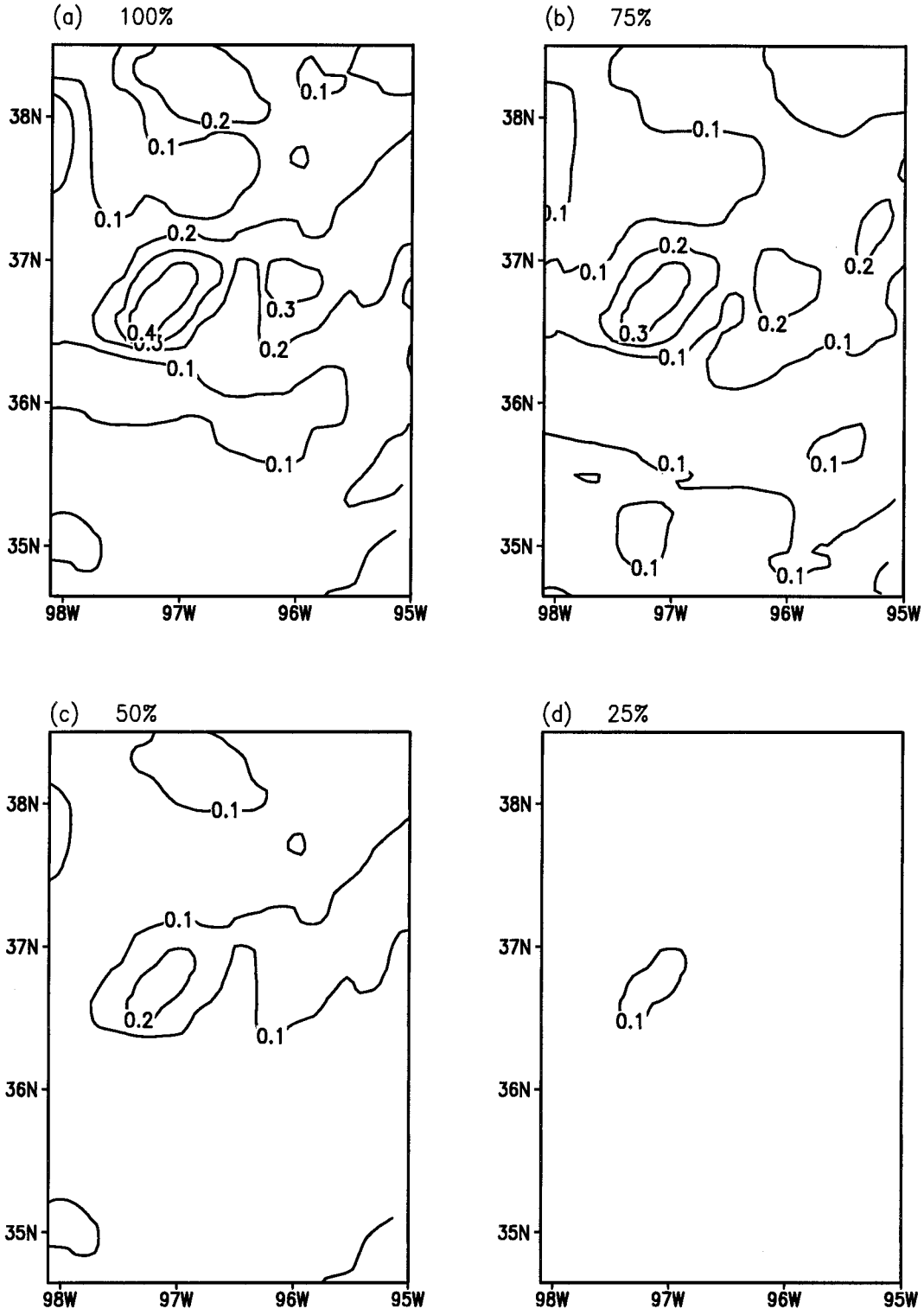


FIG. 3. Initial volumetric soil moisture for the (a) 100%, (b) 75%, (c) 50%, and (d) 25% cases. The contour interval is 0.1.

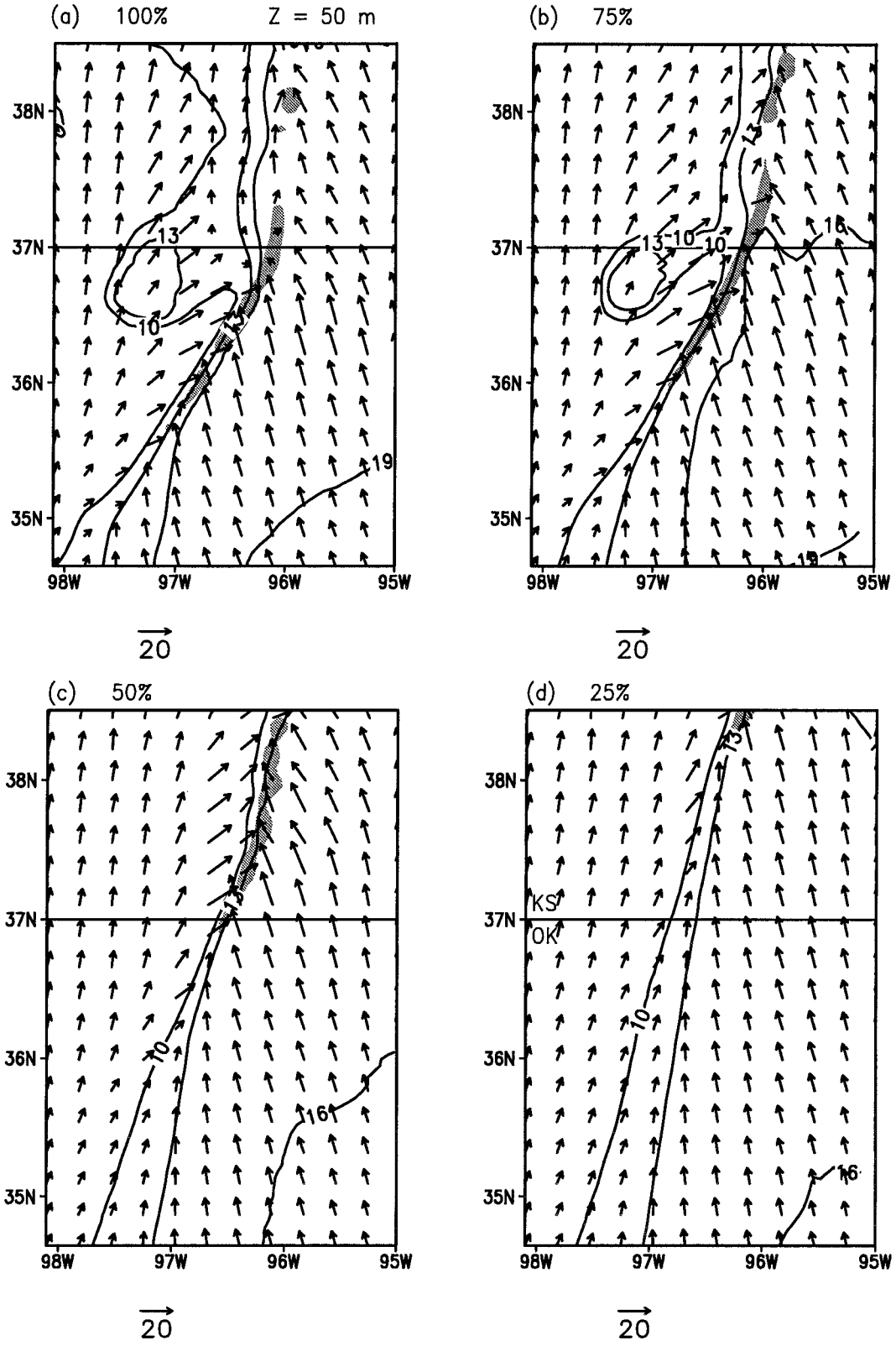


FIG. 4. Horizontal wind vectors and water vapor mixing ratio (every 3 g kg$^{-1}$) at 50 m for the (a) 100%, (b) 75%, (c) 50%, and (d) 25% cases at 0000 UTC 27 Apr 1991. Vertical motion at 4831 m greater than 5 m s$^{-1}$ is shaded.

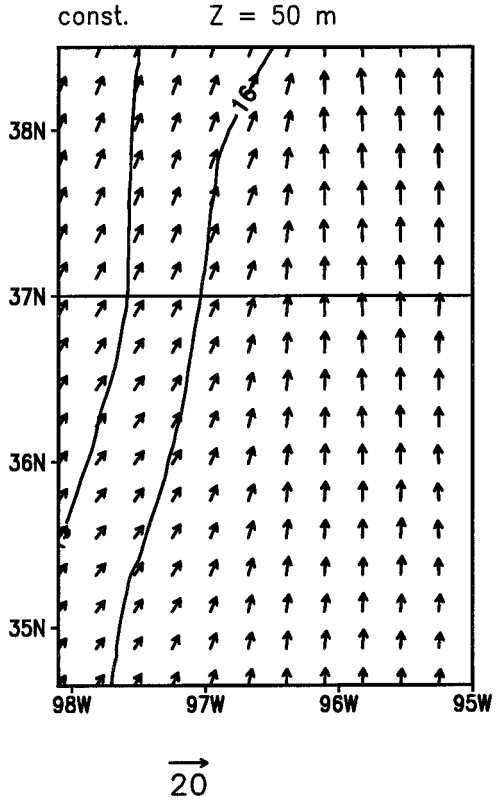


FIG. 5. Same as Fig. 4 but for the constant soil moisture simulation.

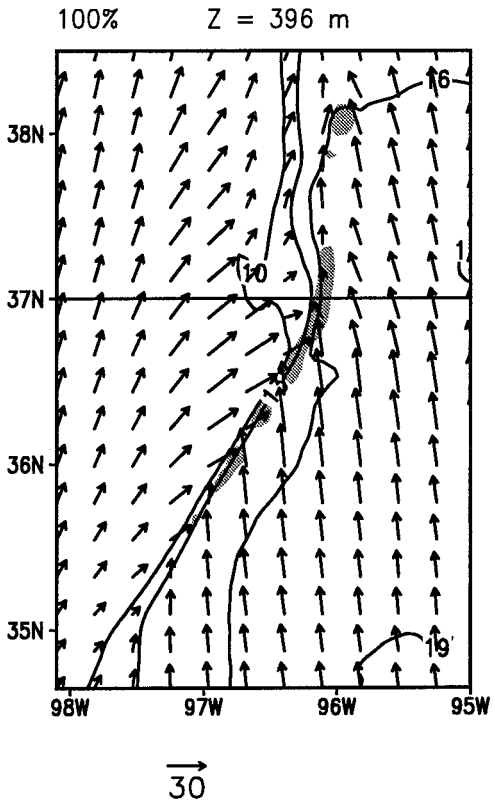


FIG. 6. Same as Fig. 4a except at 396 m.

moisture produced no dryline even though variations in terrain elevation and a larger-scale moisture gradient were present.

Sections 2 contains a description of the mesoscale model that was used for this study. Observations provide evidence that some tornadic thunderstorms on 26 April 1991 were traced back to the dryline. This is discussed further in section 3. The computational methodology is found in section 4, followed by the results from the simulations in section 5. This section also contains an analysis of the dynamics of the dryline. A discussion of the results is found in section 6. The summary and conclusions are in section 7.

## 2. Model description

The numerical model used for the dryline simulations was version 3b, of RAMS developed at Colorado State University (Pielke et al. 1992). The following features of the model were used.

- Prognostic variables are the three components of momentum, $u$, $v$, and $w$, perturbation Exner function $\pi^*$, total water $r_t$, and ice-liquid potential temperature $\theta_{il}$ (Tripoli and Cotton 1981, 1982, 1989a,b).
- Exner function tendencies used to update the momentum variables were computed using a time-split scheme, similar to Klemp and Wilhelmson (1978).
- The model was nonhydrostatic and compressible (Tripoli and Cotton 1986).
- Hybrid time step scheme: Momentum was advanced using a leapfrog scheme while scalars were advanced using a forward scheme. Both used second-order advection.
- Vertical and horizontal turbulence was parameterized using a Smagorinsky deformation-based eddy viscosity (Smagorinsky 1963) with stability modifications (Lilly 1962).
- Parameterized surface fuxes of heat, moisture, and momentum were used (Louis 1979).
- The horizontal winds at the lowest model level are reduced by an imposed drag. This produced a quasi-no-slip lower boundary.
- A terrain-following sigma coordinate system was included (Tripoli and Cotton 1981).
- Two-way interactive moving nested grids were used (Clark and Farley 1984; Walko et al. 1995).
- An Arakawa fully staggered C grid was included (Arakawa and Lamb 1981).
- A Mahrer–Pielke radiation scheme (Mahrer and Pielke 1977) for both longwave and shortwave radiation, with longitudinal variations of shortwave irradiance, was used. Radiation tendencies were recalculated every 900 s.
- A soil model extended 50 cm below ground using 11 prognostic levels (Tremback and Kessler 1985). The

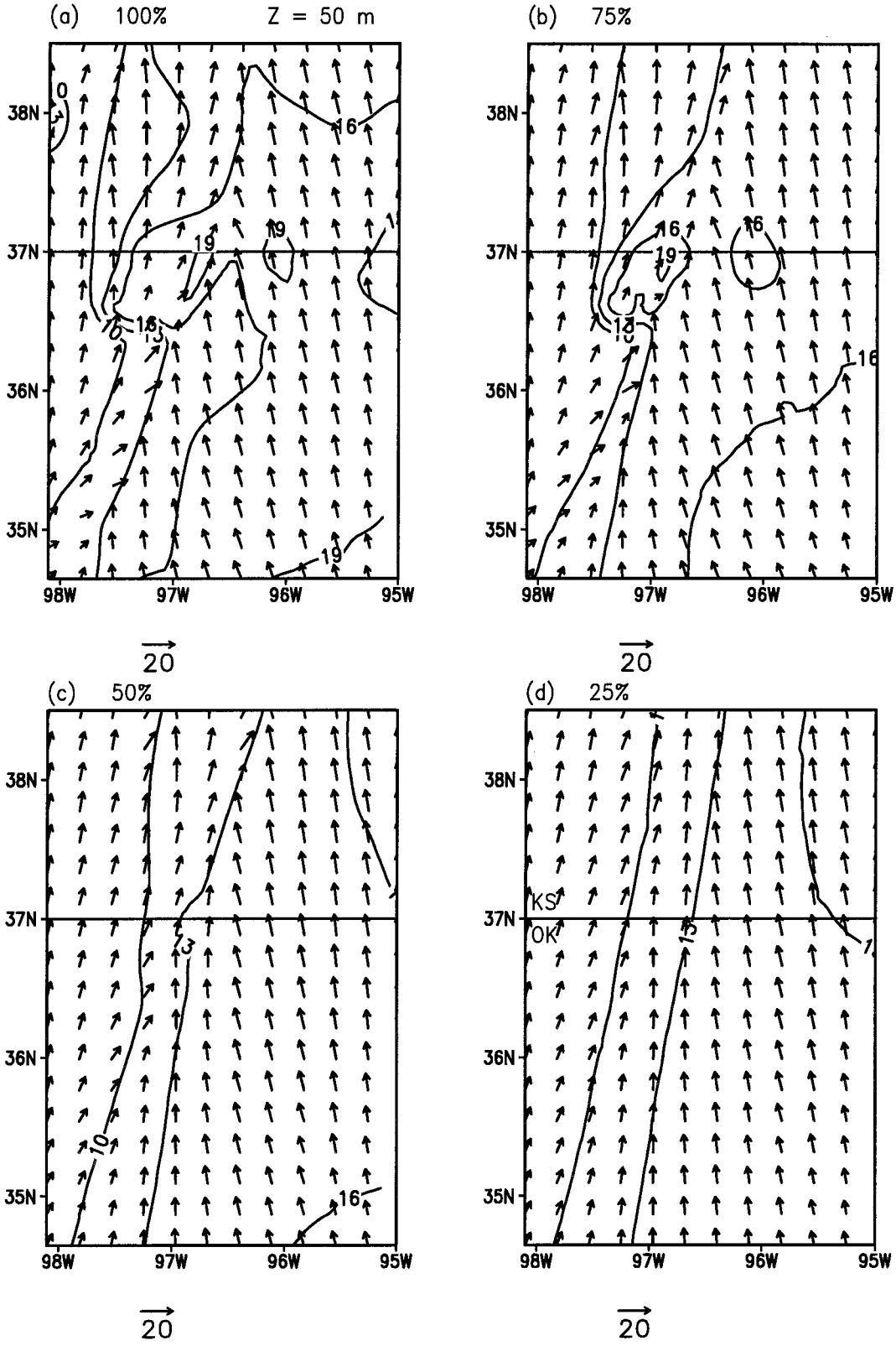


FIG. 7. Same as Fig. 4 except at 2200 UTC.

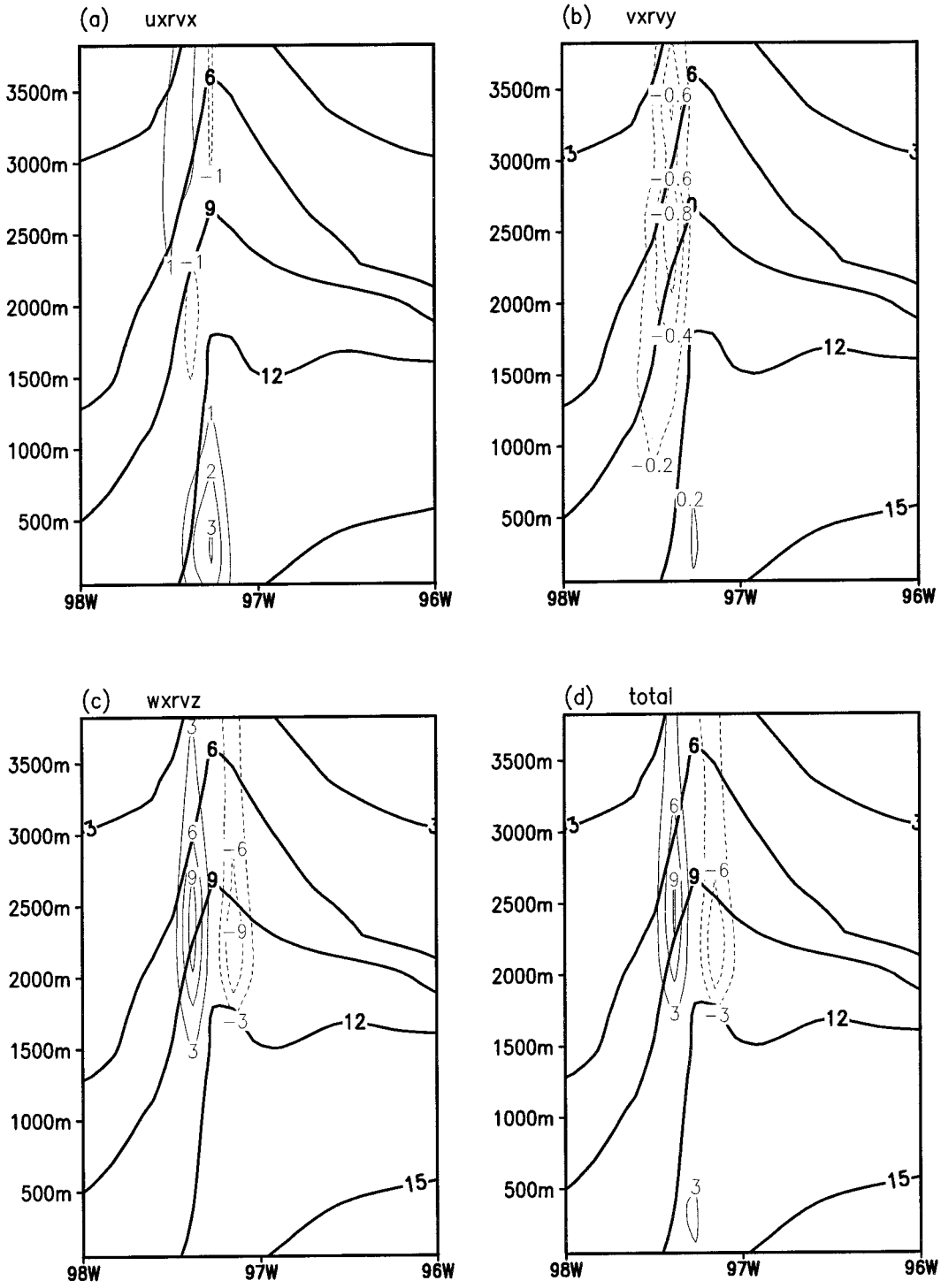


FIG. 8. Vertical cross section at 36°N of (a) uxrvx, (b) vxrvy, (c) wxrvz, and (d) total $F_x$ at 2200 UTC (thin contours). All values have been multiplied by $10^{10}$ in this and the following figures. Thick contours represent the water vapor mixing ratio (every 3 g kg$^{-1}$).

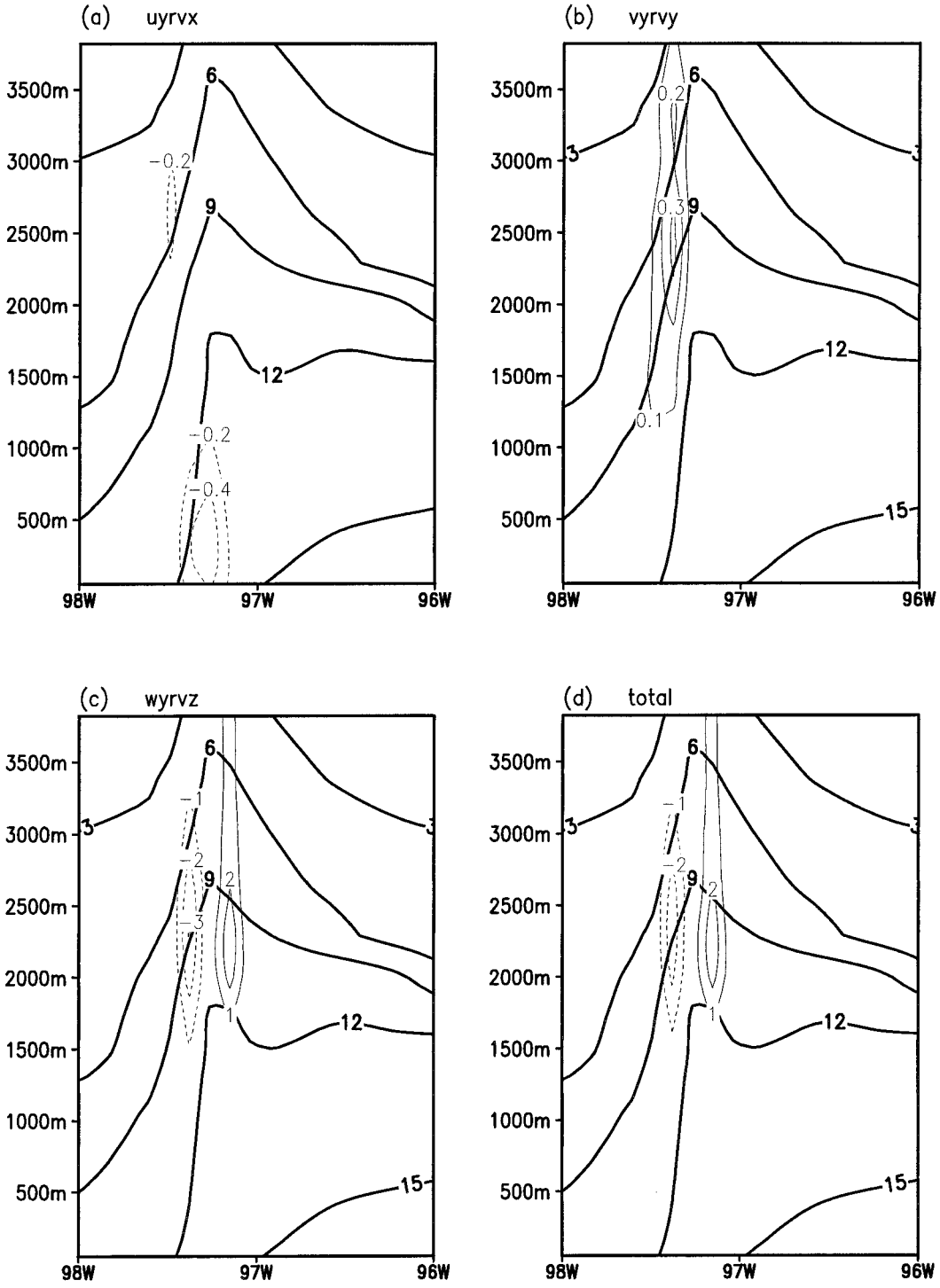


FIG. 9. Vertical cross section at 36°N of (a) uyrvx, (b) vyrvy, (c) wyrvz, and (d) total $F_y$ at 2200 UTC (thin contours). Thick contours represent the water vapor mixing ratio (every 3 g kg$^{-1}$).

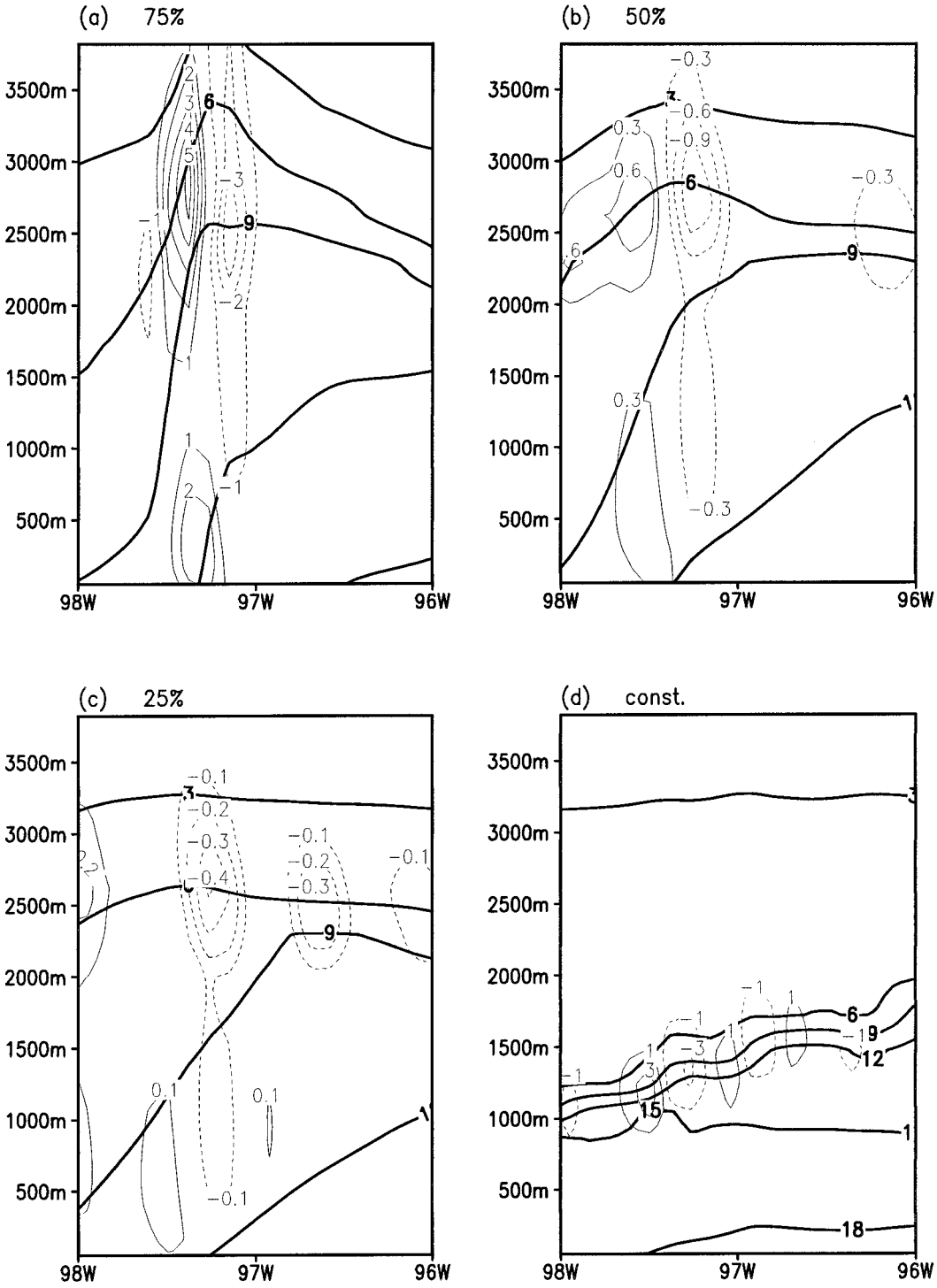


FIG. 10. Vertical cross section at 36°N of $F_x$ (thin contours) for the (a) 75%, (b) 50%, (c) 25%, and (d) constant soil moisture cases at 2200 UTC. Thick contours represent the water vapor mixing ratio (every 3 g kg$^{-1}$).

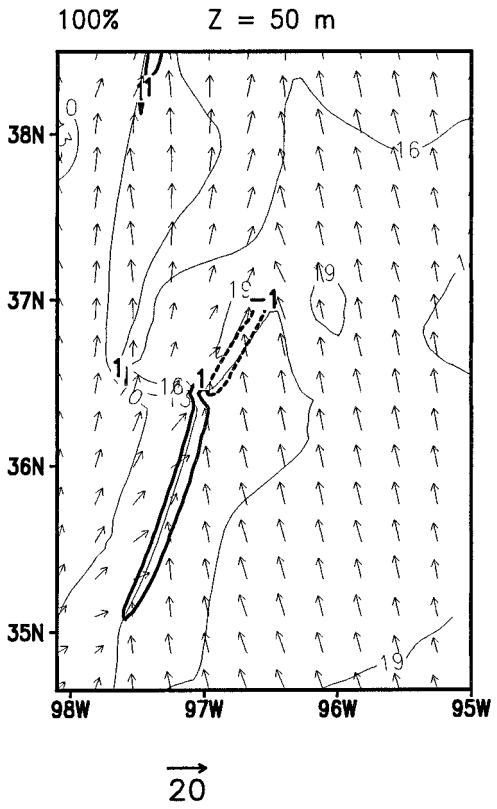


FIG. 11. Horizontal winds, water vapor mixing ratio (thin contours), and $F_x$ (thick contours) at 2200 UTC. The $F_x$ values of $-1.0$ and 1.0 are the only ones depicted for clarity.

soil type used was sandy clay loam throughout the model domain. As the model was advanced, soil moisture at the ground was reduced due to the flux of moisture upward.

- A vegetation model was included (Avissar and Pielke 1989), which was run using variable vegetation types (Loveland et al. 1991) on all three grids.
- A bulk microphysical scheme that included the following hydrometeor species: cloud water, rain, aggregates, graupel, hail, snow, and pristine ice (Walko et al. 1995). Mixing ratios were predicted for these species, except for pristine ice, where both concentration and mixing ratio were predicted, and cloud droplets, where the mixing ratio was diagnosed.

If the reader wishes to delve deeper into the model design, the following papers may prove useful: Tripoli and Cotton (1981), Cotton et al. (1986), Tremback et al. (1985), Tripoli (1986), Pielke et al. (1992), and Walko et al. (1995).

## 3. Observations

At 1800 UTC the National Centers for Environmental Prediction (NCEP) surface analysis indicated a dryline over central Kansas that extended southward over western Oklahoma. A comparison with *Geostationary Operational Environmental Satellite-7* visible imagery at 1746 UTC showed that the dryline was denoted as a cloud/no-cloud boundary, with a widespread broken cloud field to the east and a cloud-free region to the west. At that time, no deep convection was evident in the imagery at the dryline or within a few hundred kilometers to the east. At 1846 UTC, deep convection began at the dryline over north-central and south-central Kansas. Convection also began over northwest Oklahoma, ahead of the dryline, and dissipated over the next few hours. At 2046 UTC, convection developed at the dryline over northwest Oklahoma and south-central Kansas. At that time a band of thunderstorms extended eastward ahead of the dryline in central Kansas. The National Meteorological Center (now operating as NCEP) 2100. UTC surface analysis aided in locating the storms relative to the dryline.

Using the 0.5° base scan reflectivity from the KOKC radar, available approximately every 15 min, dryline-initiated convection could be traced. One storm formed at 2106 UTC in northwest Alfalfa County, Oklahoma, and moved northeastward into southern Sedgwick County, Kansas, by 2316 UTC. This storm produced an F5 tornado that touched down at 2305 UTC and was on the ground for 65 min while passing near Wichita, Kansas. Farther to the southeast, a separate storm produced three tornadoes: an F4 in Cowley County, an F3 farther northeast in Elk County, and an F3 in east Greenwood and northwest Woodson Counties in Kansas. This storm was also traced back to eastern Major County, in Oklahoma, where it was linked to the dryline at 2106 UTC. At 2316 UTC, a third storm was located over northeast Garber County, Oklahoma. This storm produced an F4/F5 tornado at 2309 UTC that was on the ground for the next 105 km. Bluestein et al. (1993) measured winds of 120–125 m $s^{-1}$ near Red Rock, Oklahoma, from this tornado. Using the KOKC radar, this storm was traced back to its genesis region, the dryline, over northeast Dewey County, Oklahoma, at 2106 UTC. Tornado tracks from the three separate storms are depicted in top of Fig. 1. There were a total of 55 tornadoes that formed from Iowa south into Texas on that day as reported in *Storm Data* (NOAA 1991).

Afternoon surface observations from 26 April 1991 indicated an approximate 20°C decrease in dewpoint temperatures from central to western Oklahoma (Fig. 1). Observed dewpoint decreases of 20°C across the western half of Oklahoma were similar to other days during the 1989 and 1991 Central Oklahoma Profiler Studies experiments (Ziegler and Hane 1993; Hane et al. 1993). A dryline, oriented approximately along a north–south line, was analyzed by NCEP along western Oklahoma and central Kansas. Winds east of the dryline were generally southeasterly with speeds ranging from 5 to 10 m $s^{-1}$. Southwesterly winds existed west of the dryline with speeds ranging from 5 to 15 m $s^{-1}$ over southwest Kansas. A cold front extended southward

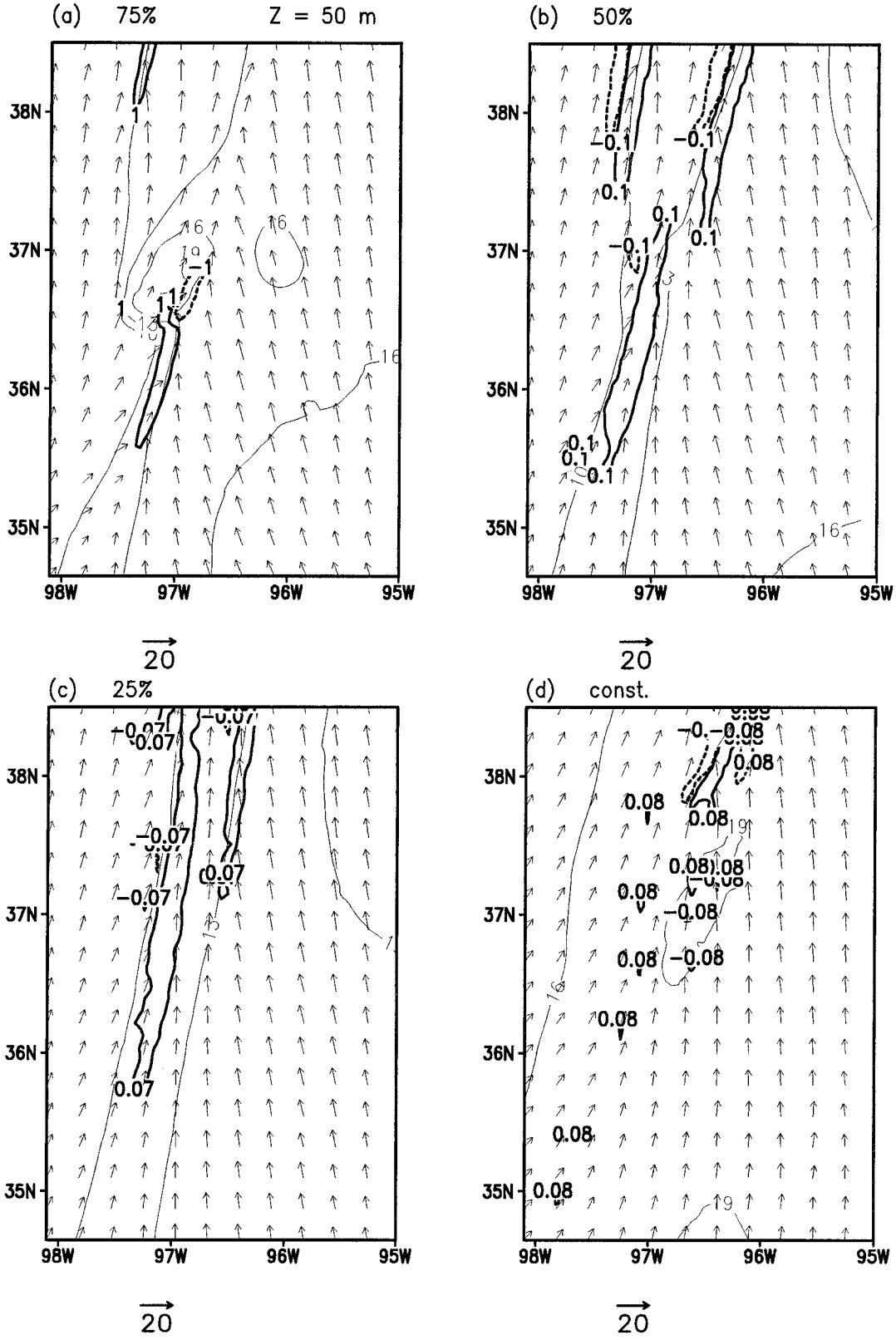


FIG. 12. Same as Fig. 11 but for the (a) 75%, (b) 50%, (c) 25%, and (d) constant soil moisture cases.

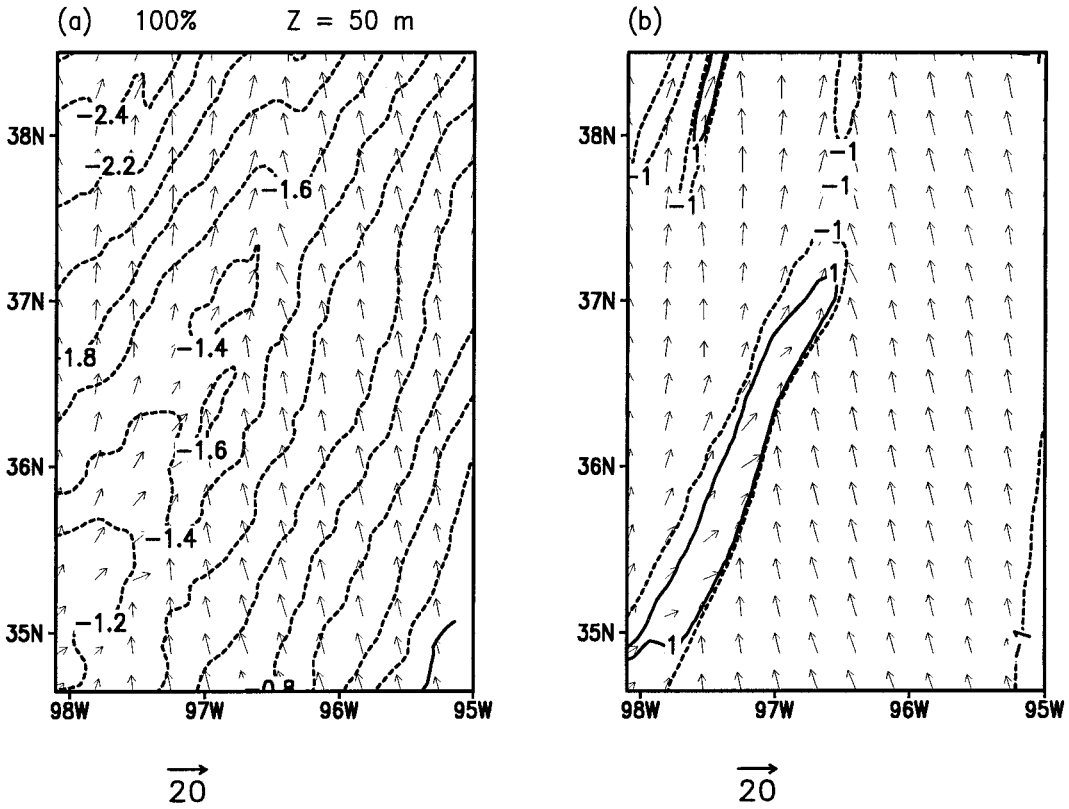


FIG. 13. Horizontal winds and (a) $\pi^*$ and (b) $-\theta_0 \partial \pi^*/\partial x$ multiplied by $10^4$ at 2200 UTC. In (b) all other contours have been omitted for clarity.

from central Nebraska, western Kansas, and through eastern sections of the Oklahoma and Texas panhandles.

Observations from 26 April 1991 indicated that a dryline could be the genesis region for the development of tornadic thunderstorms. Such storms have the potential to produce widespread damage. High impact weather of this type is important to the forecaster and the general public. Knowing when a dryline will form and trigger thunderstorms is a difficult forecasting problem.

## 4. Computational methodology

The simulations were initialized with standard 1200 UTC synoptic data on 26 April 1991. This included rawinsondes, surface observations, and NCEP Global Tropospheric Analysis which contains the 2.5° gridded winds, temperature, and moisture on pressure surfaces from the initial fields of the Aviation Model. All simulations contained a total of three, two-way, interactive grids (Fig. 2). Horizontal grid spacing used was 75, 25, and 5 km for grids one through three, respectively. The vertical grid spacing started at 100 m and was increased using a stretching ratio of 1.1. The model top was just over 23 km. All three grids were initialized at 1200 UTC and integrated to 0000 UTC 27 April 1991. During the simulations, the prognostic variables on the lateral boundaries of the outermost grid were nudged to interpolated analyses. Variables at the top boundaries were nudged on all three grids. Nudging on the top boundaries used a linear interpolation scheme between the initialization at 1200 UTC and the following synoptic analysis at 0000 UTC. The simulation also used a 30-s topographic dataset on all three grids.

The soil moisture was initialized on the first two grids using a technique based on the antecedent precipitation index (Wetzel and Chang 1988). This procedure uses 3 months of archived hourly station precipitation reports in the continental United States prior to model start time. Precipitation values were weighted more if the dates of the station reports were closer to the model start time. Soil moisture on grid 3 was interpolated from grid 2.

The first simulation used the unaltered soil moisture values derived from the above method and will be referred to as the 100% case. Three other simulations were conducted in which the soil moisture was reduced from the 100% case by multiplying soil moisture values by 0.75, 0.50, and 0.25, respectively. Those cases are referred to as the 75%, 50%, and 25% cases, respectively (Fig. 3). The soil moisture profile used in the last simulation was initialized horizontally constant with a value of 0.21 (soil moisture is a dimensionless quantity that measures the volume of water per volume of water at soil saturation). This value is approximately an average of that used in the 100% case.

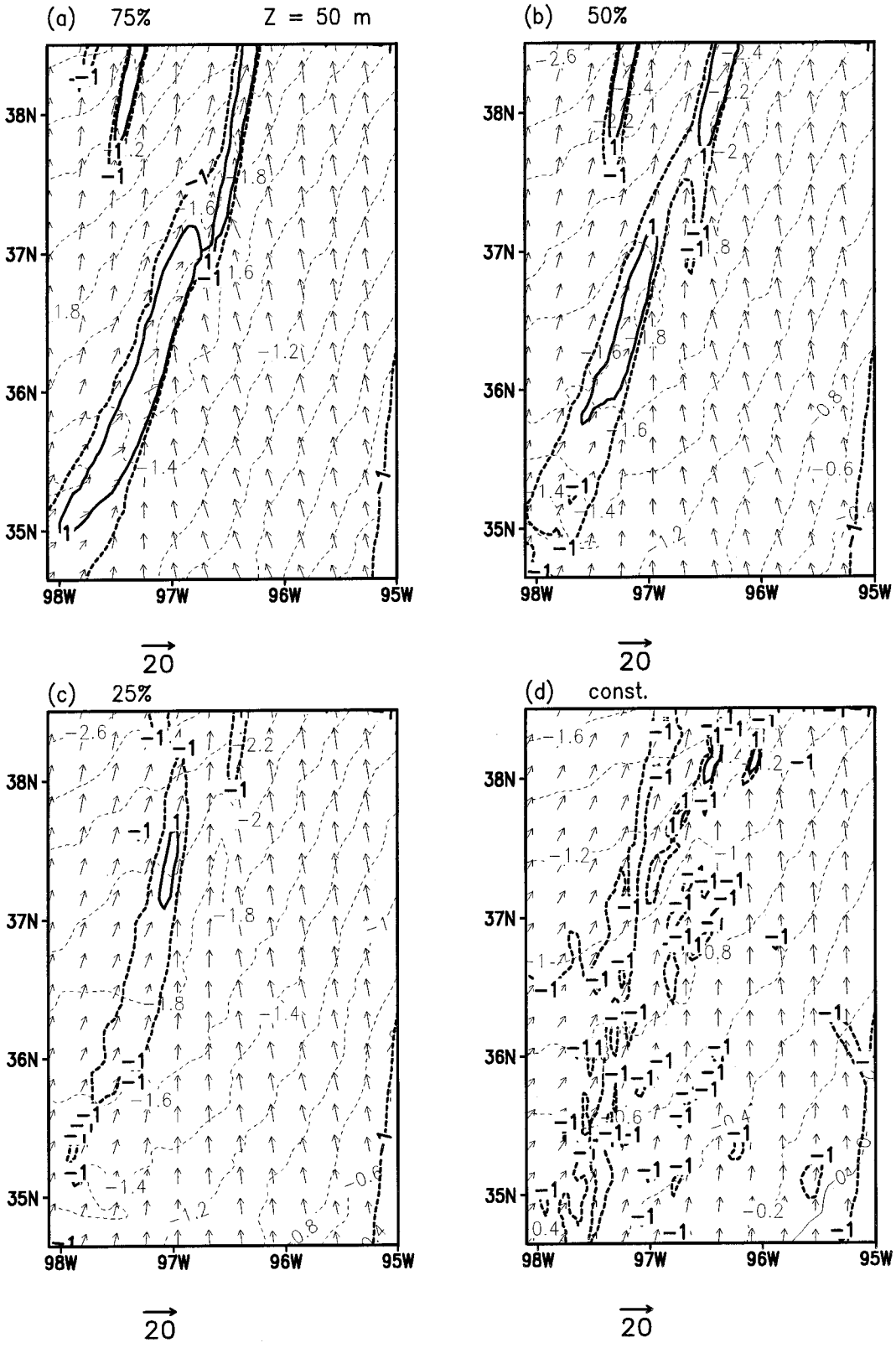


FIG. 14. Horizontal winds, $\pi^*$ (thin contours), and $-\theta_0 \partial \pi^*/\partial x$ (thick contours) multiplied by $10^4$ for the (a) 75%, (b) 50%, (c) 25%, and (d) constant soil moisture cases at 2200 UTC.

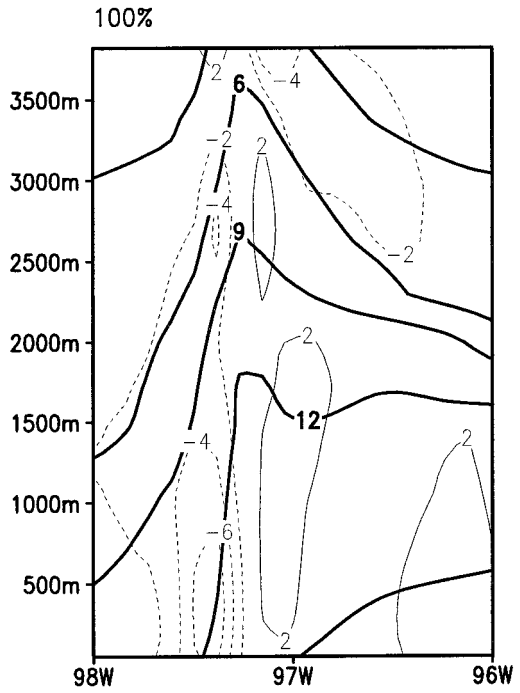


FIG. 15. Vertical cross section at 36°N of the solenoidal forcing ($-\partial B/\partial x$) multiplied by $10^6$ (thin contours) and water vapor mixing ratio (thick contours) at 2200 UTC.

## 5. Simulated dryline dynamics

While the simulation advanced from 1200 UTC there was no evidence of dryline formation, that is, an increase of the magnitude of $\nabla_h r_v$. At approximately 1900 UTC low-level convergence and the magnitude of $\nabla_h r_v$ increased relatively quickly. Soon after 2200 UTC convection, extending throughout the depth of the troposphere, developed along the dryline for the 100% case. Simulated convection did develop along the dryline for some of the other cases and is denoted by the shaded region at 0000 UTC 27 April 1991 in Fig. 4. At the same time the water vapor field, at 50 m, for the simulation with constant soil moisture is depicted in Fig. 5. As can be seen in Fig. 5, no dryline nor convection developed in that case. As a result, the simulated drylines will be analyzed prior to the development of cumulus convection, 2200 UTC, in grid 3.

There were regions of local maxima in the water vapor field located over north-central Oklahoma in Figs. 4a and 4b. These developed in response to relatively large latent heat fluxes (compared to nearby regions) from the wet soil below. Although the local maximum of soil moisture was present in the 50% and 25% cases (Figs. 3c,d), the latent heat fluxes were not large enough to noticably increase the water vapor mixing ratio at 50 m (Figs. 4c,d). The modification of the near-surface water vapor field by the underlying wet soil was confined to the lowest few hundred meters. A reproduction of Fig. 4a at 396 m shows a small region of enhanced values of $r_v$ along the Oklahoma and Kansas border (Fig. 6).

Processes governing dryline morphology will be examined prior to convective development. This will assure that any possible influence between the dryline and convective elements is removed. Winds and water vapor mixing ratios near the surface at 2200 UTC are shown in Fig. 7. A comparison between Fig. 7 and Fig. 4 indicated that the magnitude of $\nabla_h r_v$ in low levels increased rapidly (relative to the first 10 simulated hours) over the 2-h period. This was most noticable in the 100%, 75%, and 50% cases.

The time rate of change in the water vapor field will be examined through frontogenetic forcing terms. Frontogenetic forcing could also be analyzed on the dewpoint field. Water vapor mixing ratios ($r_v$), however, were chosen because they are an absolute measure of water vapor in the atmosphere. The material derivative of $\nabla_h r_v$ can be expressed as

$$\frac{D(\nabla_h r_v)}{Dt} = F_x \mathbf{e}_x + F_y \mathbf{e}_y, \tag{1}$$

where $\mathbf{e}_x$ and $\mathbf{e}_y$ are unit vectors while

$$F_x = \left[\frac{\partial}{\partial x}\left(\frac{Dr_v}{Dt}\right) - \frac{\partial u}{\partial x}\frac{\partial r_v}{\partial x} - \frac{\partial v}{\partial x}\frac{\partial r_v}{\partial y} - \frac{\partial w}{\partial x}\frac{\partial r_v}{\partial z}\right] \quad \text{and} \tag{2}$$

$$F_y = \left[\frac{\partial}{\partial y}\left(\frac{Dr_v}{Dt}\right) - \frac{\partial u}{\partial y}\frac{\partial r_v}{\partial x} - \frac{\partial v}{\partial y}\frac{\partial r_v}{\partial y} - \frac{\partial w}{\partial y}\frac{\partial r_v}{\partial z}\right]. \tag{3}$$

Following Ziegler et al. (1995), the first term on the right-hand side of Eqs. (2) and (3) will not be analyzed since the soil moisture gradients existed on a scale larger than the width of the dryline. The remaining terms will be analyzed for the 100% case and will be denoted as uxrvx, vxrvy, wxrvz in Eq. (2) and uyrvx, vyrvy, wyrvz in Eq. (3), respectively. This was done within an east–west vertical cross section at 36°N.

Terms composing $F_x$ are displayed in Fig. 8. The first term, uxrvx, maximized in the lowest 1500 m and increased the water vapor gradient (Fig. 8a). The second term, vxrvy, was weakly frontogenetic in the lowest 500 m (Fig. 8b) compared to uxrvx at the same location. Above 500 m vxrvy acted to reduce the eastward component of $\nabla_h r_v$. Values of the third term, wxrvz, indicated it had a larger influence on the water vapor field, compared to the first two terms, between approximately 1500–3500 m (Fig. 8c). Physically this term represents the turning of the water vapor isohumes into the vertical by the updraft associated with the developing dryline. The region of the wxrvz positive and negaitve couplet acted to increase $\nabla_h r_v$. Where wxrvz was positive/negative $\nabla_h r_v$ had an eastward/westward component. This resulted in an increase of the horizontal gradient of $r_v$ in both locations within that layer. The net effect (Fig. 8d) was a frontogenetic partitioning between the convergent term uxrvx, from the surface and 1500 m, and the tilting term wxrvz, between 1500 and 3500 m.

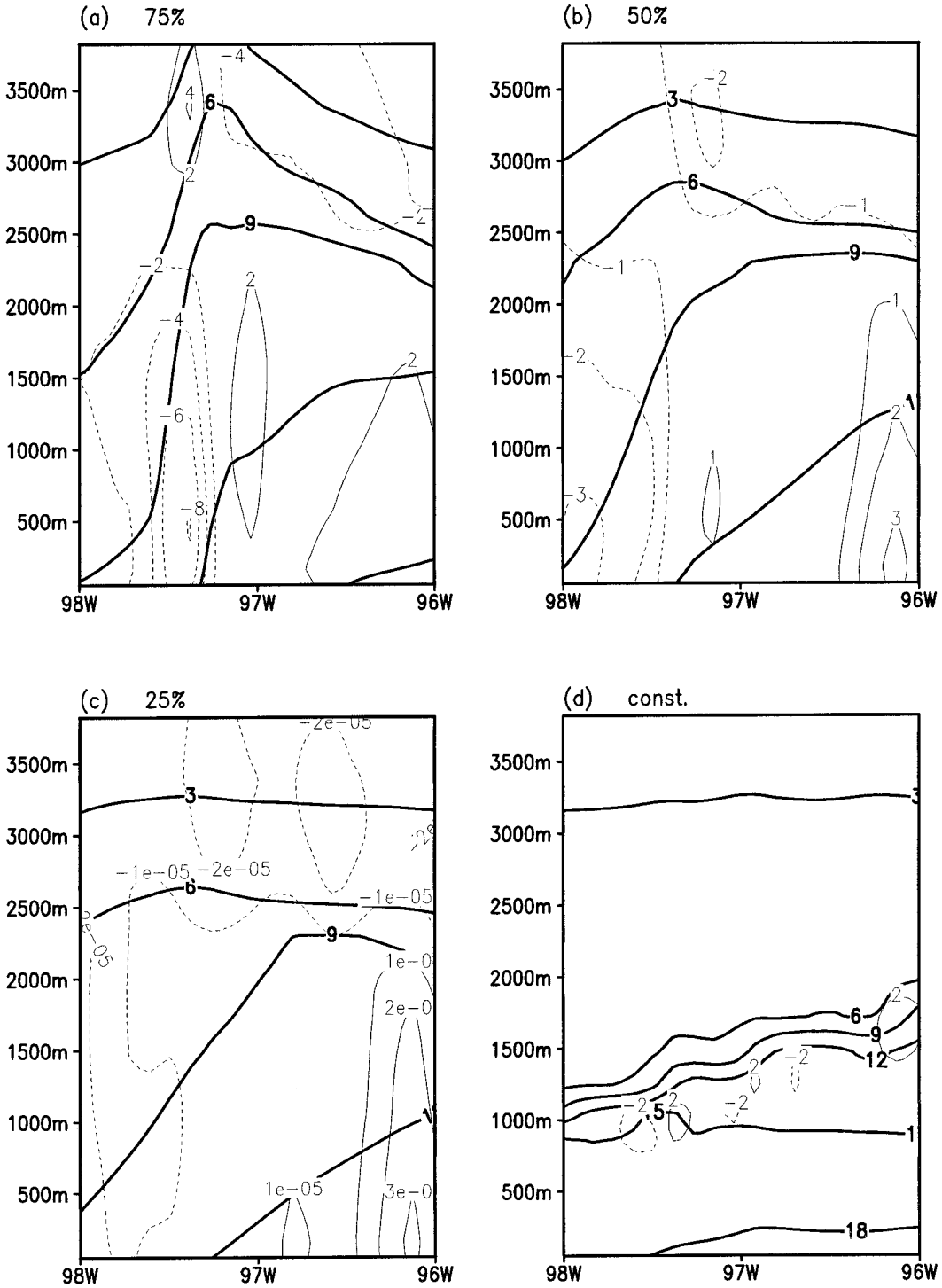


FIG. 16. Same as Fig. 15 but for the (a) 75%, (b) 50%, (c) 25%, and (d) constant soil moisture cases.

In a similar manner, the terms composing $F_y$ are shown in Fig. 9. Results of that term show that both the southward and northward components of $\nabla_h r_v$ were increased by the tilting term wyrvz from approximately 1500 to 3500 m (Fig. 9d). There was a relatively small frontolytic effect in the lowest 1000 m by the uyrvx term (Fig. 9a). Also the magnitude of $F_x$ was approximately a factor of 3 larger than $F_y$. These results suggest that processes governing the horizontal gradient of the water vapor field were generally in the east–west di-

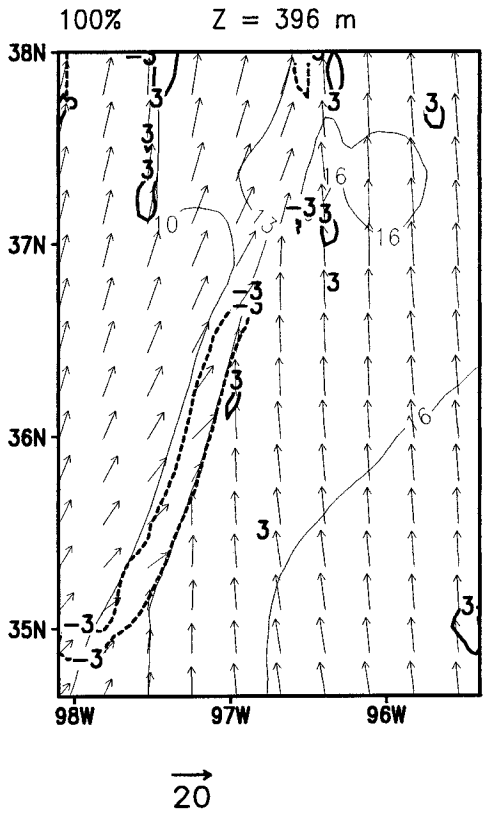


FIG. 17. Horizontal winds, water vapor mixing ratio (thin contours), and the solenoidal tendency (thick contours) multiplied by $10^6$. All other contours of the solenoidal field have been omitted for clarity.

rection. As such only the $F_x$ term was analyzed for the four other simulations (Fig. 10). As the soil moisture was reduced there was a successive reduction of the convergent/tilting forcing from the 75% to 25% cases. The constant soil moisture case showed no evidence of dryline formation through frontogenetic forcing.

The low-level water vapor field experienced frontogenesis along a convergence zone for the 100% case (Fig. 11). A region where the values of forcing were negative existed near the center of Fig. 11. This was caused by the reversal of the horizontal water vapor gradient that was associated with the low-level maximum in $r_v$ above the moist soil (Fig. 4a). Although the values of $F_x$ are negative they still represented frontogenesis since $\nabla_h r_v$ had a westward pointing component. A similar profile existed for the 75% case except the horizontal extent was smaller (Fig. 12a). As in Fig. 11 there was a general reduction in the values of $F_x$ for the 50% and 25% cases (Figs. 12b,c). For the constant soil moisture case there was weaker forcing, relative to the 100% and 75% cases. The forcing was along the confluent zone where the southwesterly winds merged with the southerly winds.

As indicated in Fig. 8a, the primary contributor to the net value of $F_x$ near the surface was the uxrvx term (Fig. 8a). Physically this means that $\nabla_h r_v$ increased over time due to the superposition of the positive water vapor gradient, $\partial r_v/\partial x > 0$, and the convergent wind field $\partial u/\partial x < 0$. This can be seen in Fig. 11 where positive frontogenetic forcing existed. An examination of Fig. 4a shows that there was veering and acceleration of the winds along 36°N from the west side of the figure to the 10.0 g kg$^{-1}$ contour. The veering was also evident at 2200 UTC in the same region (Fig. 11). That aspect of the winds suggests the existence of a trough in the pressure field along the convergence zone. Figure 13a indicates that a trough in the perturbation $\pi$ field did exist. The veering winds existed within a region that was characterized by an eastward acceleration (Fig. 13b), $-\theta_0 \partial \pi^*/\partial x > 0$, generated by the $\pi^*$ field. As soil moisture values decreased so did the extent of the area that experienced an eastward acceleration (Fig. 14). No eastward acceleration of the low-level winds was evident at 2200 UTC for the constant soil moisture case (Fig. 14d).

Another possible way to explain the eastward acceleration of the winds is through the existence of vertically oriented thermally driven solenoids. To test for the existence of baroclinicity along the developing dryline, the gradient of the simulated buoyancy field, $-\partial B/\partial x$, was computed. Model buoyancy is defined as $B = (\theta^*/\theta_0 - r_c)g$. In this expression $r_c$ and $g$ represents the total water condensate mixing ratio and the gravitational acceleration, respectively. The other two variables represent the reference state potential temperature, $\theta_0$, and perturbation potential temperature, $\theta^*$. Results of this calculation along 36°N for the 100% case supports the existence of two solenoids of opposite signs (Fig. 15). Both solenoids acted to increase the low-level convergence and aid in the development of the dryline. As a consequence of mass continuity, the increase of low-level convergence implied an increase of vertical motion. (This may have important implications to the study of convective initiation along the dryline. Although it is an important topic, it is outside the scope of this study and will be contained in a future manuscript.) Solenoids were evident in the 75% case (Fig. 16a) and to a lesser extent in the 50% case (Fig. 16b). Solenoids were essentially absent in the other two cases (Figs. 16c,d).

An examination of Fig. 15 shows that the magnitude of the low-level solenoid forcing maximized a few hundred meters above the ground for the 100% case. At 396 m the solenoidal forcing (Fig. 17) extended generally over the same region as did the eastward acceleration generated by the $\pi^*$ gradient (Fig. 13b). A similar relationship between the solenoid forcing and the eastward acceleration was evident in the other cases (cf. Figs. 18 and 14). Also indicated in Fig. 18 is the overall reduction of the solenoid forcing as the soil moisture was reduced.

## 6. Discussion

Past research on dryline movement has examined the relatively rapid eastward progression of the 9.0 g kg$^{-1}$

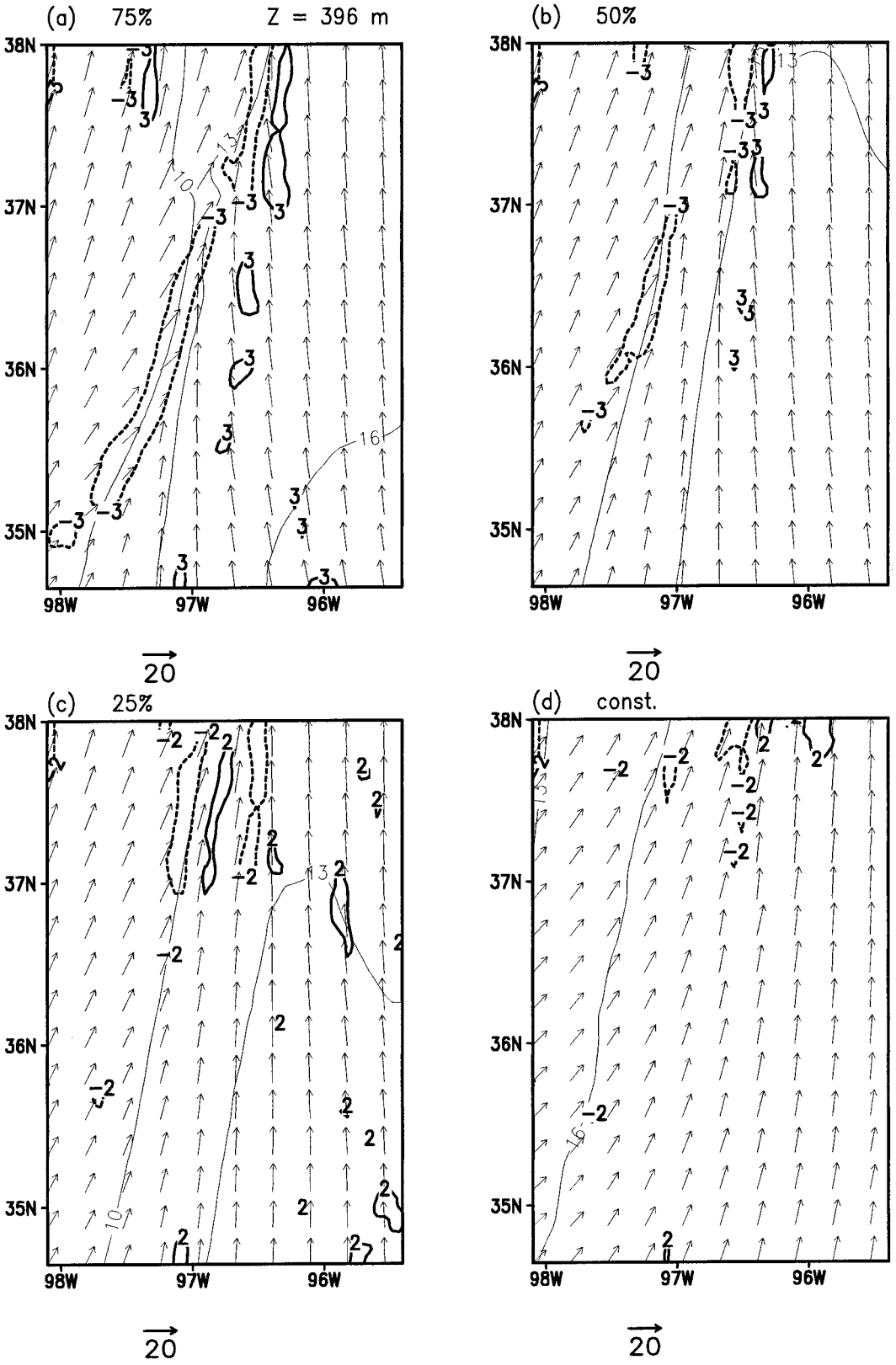


FIG. 18. Same as Fig. 17 but for the (a) 75%, (b) 50%, (c) 25%, and (d) constant soil moisture cases.

water vapor mixing ratio contour. This contour was used to denote the location of the dryline in some studies. A combination of the downward sloping terrain toward the east, a thinning of the moist layer toward the west, and horizontal variations of vertical turbulent mixing have been suggested to explain dryline movement.

Except for the constant soil moisture simulation, the 9.0 g kg$^{-1}$ water vapor mixing ratio contour moved east a few hundred kilometers prior to 2200 UTC. At that time $\nabla_h r_v$ was still relatively small compared to 0000 UTC for the 100%, 75%, and portions of the 50% cases. Even though the 9.0 g kg$^{-1}$ water vapor contour moved east in the 25% case, no further increase of $\nabla_h r_v$ occurred from 2200 to 0000 UTC. Dryline development and movement of the 9.0 g kg$^{-1}$ isohume were essentially absent in the constant soil moisture case. In both of these cases solenoids were also absent.

These results suggest that the proposed mechanism for the movement of the 9.0 g kg$^{-1}$ contour did not aid in the increase of the magnitude of $\nabla_h r_v$ from 2200 to 0000 UTC in some of the simulations presented here. Results from this study suggest that the continued increase of the magnitude of $\nabla_h r_v$, from 2200 to 0000 UTC, resulted from two related processes. First was the thermally driven solenoids that aided in the eastward acceleration of the winds at the dry side of the dryline. The second process was frontogenetic forcing of the water vapor field superimposed on the convergent wind field within the lowest 1000 m.

Future work will address how the magnitude and horizontal variations of soil moisture influence the low-level pressure field, solenoids, and frontogenesis along the dryline. Regions where the soil moisture was larger resulted in a reduction of sensible heating and an increase of latent heating. The total flux was essentially constant for all simulations. The difference was in the partitioning of the total flux into sensible and latent heat fluxes.

## 7. Summary and conclusions

Drylines are a region where thunderstorms can develop during the spring and early summer. Some of these storms may produce hazardous weather and damage to property. For this reason understanding the movement and the relatively rapid increase of $\nabla_h r_v$ at the dryline are important to forecasters.

Two-dimensional studies have shown that dryline movement, denoted by the 9.0 g kg$^{-1}$ isohmue, can be attributed to vertical turbulent mixing of the shallow portion of the moist layer above sloping terrain. They have also been used to show the importance of horizontally varying soil moisture on dryline development through the frontogenesis process. Three-dimensional simulations have also demonstrated an influence of horizontally varying soil moisture, and other surface characteristics, on dryline evolution.

In this study a three-dimensional model was used to provide more experiments that demonstrate the sensitivity of dryline evolution to soil moisture. Five simulations were conducted in which only soil moisture was changed. Results suggest that the evolution of some drylines may be influenced by horizontal soil moisture variations. This may have an important consequence. The ability of a mesoscale model to accurately simulate dryline evolution in a regional setting (research or forecasting) may be greatly reduced through the use of constant soil moisture.

Results of this study also suggest that dryline morphology may be a two-step process. The first is the increase of the larger-scale eastward gradient of moisture through the erosion of the shallow moist layer by turbulent mixing. The second is the relatively rapid increase of the magnitude of the $\nabla_h r_v$ through vertically oriented solenoids and frontogenetic forcing. Convective initiation at the dryline may be related to the magnitude of the second step.

Future work will examine the relationship between soil moisture, latent and sensible heat fluxes, and dryline evolution. Currently a fourth grid has been spawned at 2000 UTC for the 100% case. This grid has horizontal grid spacings of 1.6 km. Several thunderstorms have developed along the dryline in a nonuniform manner. Results from this grid will be used to study convective initiation along the simulated dryline.

*Acknowledgments.* This material is based on work supported by the National Oceanic and Atmospheric Administration under Grant NA67RJ0152. The author would like to thank Dr. Mark DeMaria and Dr. John Knaff for their helpful comments to improve this manuscript.

## REFERENCES

Anthes, R. A., Y. H. Kuo, S. G. Benjamin, and Y.-F. Li, 1982: The evolution of the mesoscale environment of severe local storms: Preliminary modeling results. *Mon. Wea. Rev.*, **110,** 1187–1213.

Arakawa, A., and V. Lamb, 1981: A potential enstrophy and energy conserving scheme for the shallow water equations. *Mon. Wea. Rev.*, **109,** 18–36.

Avissar, R., and R. A. Pielke, 1989: A parameterization of heterogeneous land surfaces for atmospheric numerical models and its impact on regional meteorology. *Mon. Wea. Rev.*, **117,** 2113–2136.

Benjamin, S. G., 1986: Some effects of surface heating and topography on the regional severe storm environment. *Mon. Wea. Rev.*, **114,** 307–343.

Bluestein, H. B., and S. S. Parker, 1993: Modes of isolated, severe convective storm formation along a dryline. *Mon. Wea. Rev.*, **121,** 1352–1374.

——, J. G. LaDue, H. Stein, D. Speheger, and W. P. Unruh, 1993: Doppler-radar measurements of the maximum wind speed in tornadoes: A comparison with the thermodynamic wind speed limit. Preprints, *17th Conf. on Severe Local Storms*, St. Louis, MO, Amer. Meteor. Soc., 277–281.

Clark, T. L., and R. D. Farley, 1984: Severe downslope windstorm calculations in two and three spacial dimensions using anelastic interactive grid nesting: A possible mechanism for gustiness. *J. Atmos. Sci.*, **41,** 329–350.

Cotton, W. R., G. J. Tripoli, R. M. Rauber, and E. A. Mulvihill, 1986: Numerical simulation of the effect of varying ice crystal nucleation rates and aggregation process on orographic snowfall. *J. Climate Appl. Meteor.,* **25,** 1658–1680.

Hane, C. E., C. L. Ziegler, and H. B. Bluestein, 1993: Investigation of the dryline and convective storms initiated along the dryline: Field experiments during COPS-91. *Bull. Amer. Meteor. Soc.,* **74,** 2133–2145.

Klemp, J. B., and R. B. Wilhelmson, 1978: The simulation of three-dimensional convective storm dynamics. *J. Atmos. Sci.,* **35,** 1070–1096.

Koch, S. E., and J. McCarthy, 1982: The evolution of an Oklahoma dryline. Part II: Boundary-layer forcing of mesoscale systems. *J. Atmos. Sci.,* **39,** 237–257.

Lanicci, J. M., T. N. Carlson, and T. T. Warner, 1987: Sensitivity of the Great Plains severe storm environment to soil moisture distribution. *Mon. Wea. Rev.,* **115,** 2660–2673.

Lilly, D. K., 1962: On the numerical simulation of buoyant convection. *Tellus,* **14,** 148–172.

Louis, J. F., 1979: A parametric model of vertical eddy fluxes in the atmosphere. *Bound.-Layer Meteor.,* **17,** 187–202.

Loveland, T. R., J. W. Merchant, D. O. Ohlen, and J. F. Brown, 1991: Development of a land-cover characteristics database for the conterminous U.S. *Photo. Eng. Remote Sens.,* **57,** 1453–1463.

Mahrer, Y., and R. A. Pielke, 1977: A numerical study of the airflow over irregular terrain. *Beitr. Phys. Atmos.,* **50,** 98–113.

McCarthy, J., and S. E. Koch, 1982: The evolution of an Oklahoma dryline. Part I: A meso-subsynoptic-scale analysis. *J. Atmos. Sci.,* **39,** 225–236.

McGuire, E. L., 1962: The vertical structure of three drylines as revealed by aircraft traverses. National Severe Storms Project Rep. 7, Kansas City, MO, 11 pp.

NOAA, 1991: *Storm Data.* Vol. 33, No. 4, p. 239.

Ogura, Y., and Y. Chen, 1977: A life history of an intense mesoscale convective storm in Oklahoma. *J. Atmos. Sci.,* **34,** 1458–1476.

Parsons, D. B., M. A. Shapiro, R. M. Hardesty, and R. J. Zamora, 1991: The finescale structure of a west Texas dryline. *Mon. Wea. Rev.,* **119,** 1242–1258.

Pielke, R. A., and Coauthors, 1992: A comprehensive meteorological modeling system—RAMS. *Meteor. Atmos. Phys.,* **49,** 69–91.

Rhea, J. O., 1966: A study of thunderstorm formtion along dry lines. *J. Appl. Meteor.,* **5,** 58–83.

Schaefer, J. T., 1974: A simulative model of dryline motion. *J. Atmos. Sci.,* **31,** 956–964.

——, 1986: The dryline. *Mesoscale Meteorology and Forecasting,* P. S. Ray, Ed., Amer. Meteor. Soc., 549–570.

Shaw, B. L., R. A. Pielke, and C. L. Ziegler, 1997: The effect of soil moisture heterogeneity on a Great Plains dry line: A numerical study. *Mon. Wea. Rev.,* **125,** 1489–1506.

Smagorinsky, J., 1963: General circulation experiments with the primitive equations. Part 1: The basic experiment. *Mon. Wea. Rev.,* **91,** 99–164

Sun, W. Y., and C. C. Wu, 1992: Formation and diurnal variation of the dryline. *J. Atmos. Sci.,* **49,** 1606–1618.

Tremback, C. J., and R. Kessler, 1985: A surface temperature and moisture parameterization for use in mesoscale numerical models. Preprints, *Seventh Conf. on Numerical Weather Prediction,* Montreal, PQ, Canada, Amer. Meteor. Soc., 355–358.

——, G. J. Tripoli, and W. R. Cotton, 1985: A regional scale atmospheric numerical model including explicit moist physics and a hydrostatic time-split scheme. Preprints, *Seventh Conf. on Numerical Weather Prediction,* Montreal, PQ, Canada, Amer. Meteor. Soc., 433–434.

Tripoli, G. J., 1986: A numerical investigation of an orogenic mesoscale convective system. Ph.D. dissertation, Atmospheric Science Paper 401, 290 pp. [Available from Dept. of Atmospheric Science, Colorado State University, Fort Collins, CO 80523.]

——, and W. R. Cotton, 1981: The use of ice-liquid water potential temperature as a thermodynamic variable in deep atmospheric models. *Mon. Wea. Rev.,* **109,** 1094–1102.

——, and ——, 1982: The Colorado State University three dimensional cloud mesoscale model, 1982. Part I: General theoretical framework and sensitivity experiments. *J. Rech. Atmos.,* **16,** 185–220.

——, and ——, 1986: An intense quasi-steady thunderstorm over mountainous terrain. Part IV: Three-dimensional numerical simulation. *J. Atmos. Sci.,* **43,** 894–912.

——, and ——, 1989a: A numerical study of an observed orogenic mesoscale convective system. Part 1: Simulated genesis and comparison with observations. *Mon. Wea. Rev.,* **117,** 273–304.

——, and ——, 1989b: A numerical study of an observed orogenic mesoscale convective system. Part 2: Analysis of governing dynamics. *Mon. Wea. Rev.,* **117,** 305–328.

Walko, R. L., W. R. Cotton, M. P. Meyers, and J. Y. Harrington, 1995: New RAMS cloud microphysics parameterization. Part I: The single moment scheme. *Atmos. Res.,* **38,** 29–62.

Wetzel, P. J., and J. T. Chang, 1988: Evapotranspiration from nonuniform surfaces: A first approach for short-term numerical weather prediction. *Mon. Wea. Rev.,* **116,** 600–621.

Ziegler, C. L., and C. E. Hane, 1993: An observed study of the dryline. *Mon. Wea. Rev.,* **121,** 1134–1151.

——, W. J. Martin, R. A. Pielke, and R. L. Walko, 1995: A modeling study of a dryline. *J. Atmos. Sci.,* **52,** 263–285.